Human Serum Albumin Dimerization Enhances S_2 Emission of Bound Cyanine IR806

Jurick Lahiri[1], Shawn Sandhu[1], Benjamin G. Levine[2], and Marcos Dantus[1,3,*]

[1] Department of Chemistry, Michigan State University, East Lansing, MI 48824, USA

[2] Institute for Advanced Computational Science and Department of Chemistry, Stony Brook University, Stony Brook, NY 11794, USA

[3] Department of Physics and Astronomy, Michigan State University, East Lansing, MI 48824, USA

* Email: dantus@chemistry.msu.edu

ABSTRACT

Cyanine molecules are important phototheranostic compounds given their high fluorescence yield in the near-infrared region of the spectrum. We report on the frequency and time-resolved spectroscopy of the S_2 state of IR806 which, upon binding to the hydrophobic pocket of human serum albumin (HSA), demonstrates enhanced emission. From excitation emission matrix spectra and electronic structure calculations, we identify the emission as one associated with a 103-degree twisted geometry state. In addition, we find that this configuration is significantly stabilized as the concentration of HSA is increased. Spectroscopic changes associated with the S_1 and S_2 states as a function of concentration, as well as anisotropy measurements, confirm the formation of HSA dimers at concentrations greater than 10 μM. These findings imply that the longer-lived S_2 state configuration can lead to more efficient phototherapy agents and cyanine S_2 spectroscopy may be a useful tool to determine the oligomerization state of HSA.

TOC Graphic

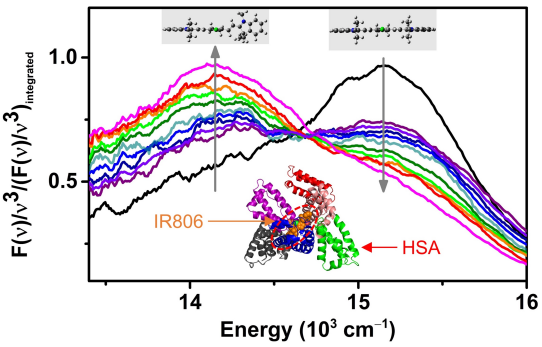

Excitation to high-lying electronic excited states usually leads to internal conversion (IC) to the lowest excited state, as postulated by Kasha.[1] Efforts to extend the lifetime of higher excited states, including increasing the solvent viscosity, have been shown to decrease the rate of IC.[2–4] The combination of viscosity and nonlinear excitation has been shown to cause changes in the S_2/S_1 population ratio that are greater than an order of magnitude.[5] Here, the protein pocket of human serum albumin (HSA) is found to stabilize the S_2 state of cyanine IR806 in a geometry that delays the excited state non-radiative dynamics, resulting in a longer S_2 excited state lifetime. As the HSA concentration increases and protein dimers form, we find increased emission due to greater constraint of the molecular structure.

Heptamethine cyanine dyes are promising phototheranostic reagents given their high fluorescent yield and generation of singlet oxygen.[6–9] IR806 (2-[2-[2-chloro-3-[2-[1,3-dihydro-3,3-dimethyl-1-(4-sulfobutyl)-2H-indol2-ylidene]-ethylidene]-1-cyclopenten-1-y1]ethenyl]3,3dimethyl)-1(4-sulfobutyl)-3H-indolium hydroxide, inner sodium salt) is a heptamethine cyanine dye capable of exhibiting extended conjugation through the polymethine group (Scheme 1a), allowing it to absorb and emit light in the IR region. IR806 is of interest due to its high extinction coefficient as well as quantum efficiency, giving it the potential to be used as a phototheranostic agent.[10–13] Extending the lifetime of the S_2 state of cyanines can lead to phototheranostic activity via two-photon excitation of the S_2 state with near-IR laser pulses.[14,15] The motivation for the use of IR806 can be derived from the similarities to the heptamethine dye IR125, also known as indocyanine green (Scheme 1b), the only near-IR FDA approved dye, which is extensively used for medical diagnostics including cardiac output measurements, liver function and ophthalmic angiography.[16–18] Previous studies involving cyanine dyes have shown that these molecules binds HSA, the most abundant protein in blood.[19–23]

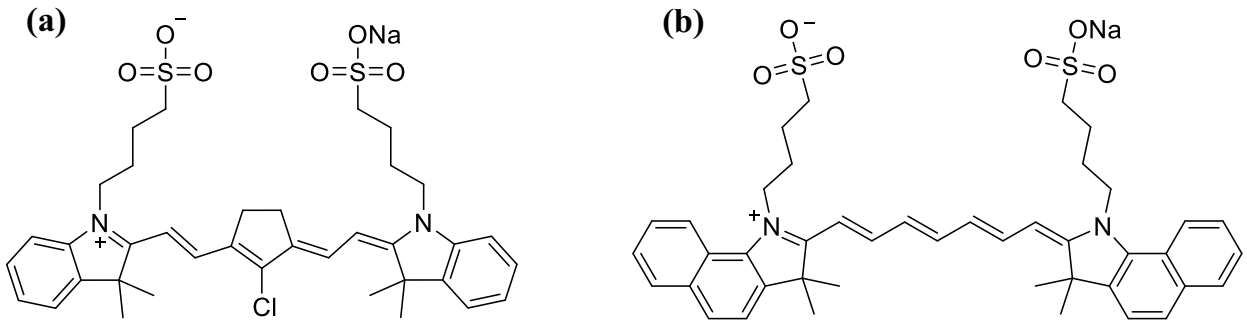

Scheme 1 Molecular structure of (a) IR806 and (b) IR125.

HSA consists of 585 amino acids with a molecular weight of 66.5 kDa.[24–26] In vivo HSA has a wide variety of functions in addition to maintaining plasma oncotic pressure, such as transporting steroids and the capability of binding to reactive oxygen species.[27–30] Thus, understanding the interactions of molecules with HSA is of great importance due to HSA's ability to allow binding and transporting a wide variety of molecules such as fatty acids, hormones, and a multitude of drugs.[31–33] X-ray crystallographic studies have shown that HSA has a heart-shaped tertiary structure, which changes to an ellipsoid in solution.[34,35] Hence, the tertiary and quaternary structure of HSA must be dependent on the overall concentration of HSA in solution, which would naturally alter the behavior of the protein. Research has shown that reversible non-bonding dimers of HSA occur in concentrations as low as 10 μM,[36,37] indicating that a significant portion of HSA could exist as dimers in the blood stream of a healthy individual where the concentration is between 526–753 μM.[25] Additionally, HSA dimers are a biomarker for oxidative stress and liver cirrhosis.[38,39] Spectroscopic agents capable of quantifying HSA dimer concentration may be of great value.

The binding of IR806 with HSA has been experimentally confirmed in Awasthi et. al.'s work.[20] The two common ligand binding sites in HSA are the hydrophobic cavities in subdomain IIA and IIIA.[19–23,40] The binding site in subdomain IIA exhibits hydrophobic interactions which are strongly influenced by interactions with the hydrophobic sections of the binding dye.

In our recent studies of the higher excited states of IR144 and IR140, we found two S_2 states which have distinctly different geometries designated as S_2^H and S_2^L.[5] The geometry of S_2^H resembles a planar structure in the polymethine chain and fluoresces at a higher frequency. The geometry of S_2^L shows a 94- and 91-degree twist in the polymethine chain, respectively, which fluoresce at a lower frequency. We find that IR806, when bound to HSA, adopts a distorted geometry. Based on spectroscopic data and calculations, we find that S_0 and S_1 states have energy minima corresponding to their planar geometries, thus the distorted geometry involves twisting distributed among several bonds. However, we find that the S_2^L state of IR806, with a 103-degree twist in the polymethine chain is stabilized when bound to HSA. This observation is supported by an increase in the S_2^L fluorescence intensity and lifetime as the concentration of HSA increases. We present evidence for spectroscopic changes in IR806 bound to HSA occurring at concentrations where HSA reversible dimers form. This finding has two important consequences. First, a longer S_2 lifetime may enable the higher energy and hence more reactive state to act as an efficient phototheranostic species. Cyanine dyes can be designed accordingly to release therapy agents upon S_2 excitation.[10–13,15] Second, the S_2 emission of IR806 shows conspicuous enhancement following HSA dimerization, in comparison to low HSA concentration. Therefore, it points to a spectroscopic method for quantifying the degree of aggregation of HSA, which has been linked to oxidative stress and liver cirrhosis.

The normalized steady-state absorption of IR806 in buffer solution is shown in Figure 1a, which shows an absorption maximum for the first electronic excited state (S_1) at 12520 cm^{-1}, accompanied by a vibronic shoulder at 13600 cm^{-1}. Keeping the IR806 concentration constant at 5 μM, we increased the concentration of HSA, which resulted in a red shift of the S_1 absorption maximum. The red shift indicates IR806 is binding to the hydrophobic IIA pocket. The 1:15 IR806-HSA solution shows a red shift of 200 cm^{-1} in comparison to the unbound dye. The extinction coefficients of these solutions are presented in the Supporting Information (SI) Fig. S1. The excitation emission matrix (EEM) spectrum of IR806 in solution is shown in Figure 1b, and the EEM for a 1:15 IR806-HSA mixture is shown in Figure 1c. The emission maximum for S_1 shows a red-shift of 160 cm^{-1} in the unbound dye compared to the IR806-HSA mixture. The EEM spectrum of IR806 reveals higher excited state emissions, which we shall label as S_2^H and S_2^L, which show excitation maxima at 16300 cm^{-1} and 14880 cm^{-1}, respectively. The corresponding emission maxima for S_2^H and S_2^L are 15290 cm^{-1} and 14130 cm^{-1}, respectively. It is worth noting that, although we are not able to identify the S_2^H and S_2^L absorption maxima from the absorption spectra, mainly because of the strong S_1 absorption, we can determine excitation maxima from the EEM spectra. The EEM spectra for all the different concentrations can be found in the SI (Figure S2).

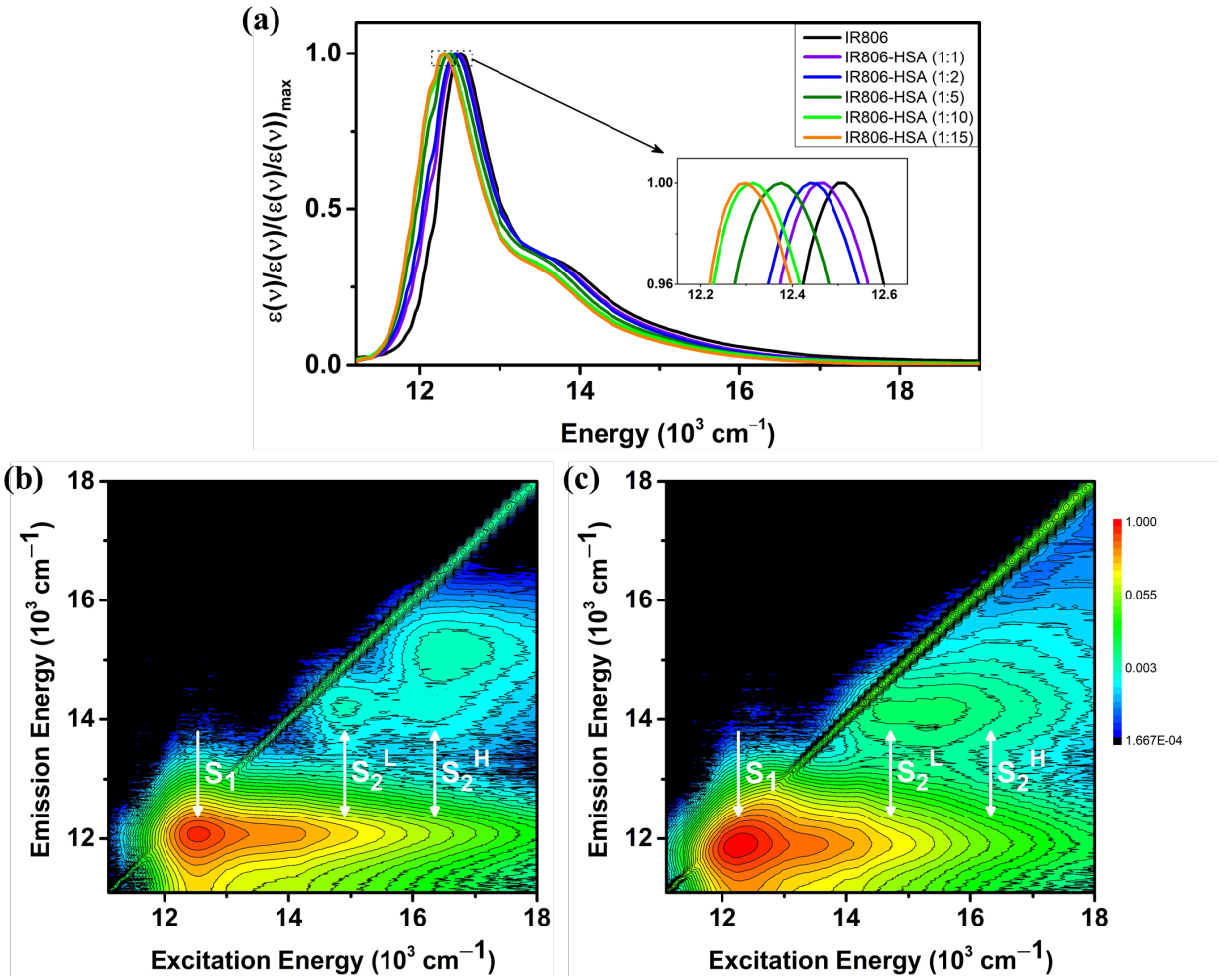

Figure 1. Steady-state absorption and fluorescence spectra. (a) Normalized absorption of IR806 and IR806-HSA samples prepared in pH 7.4 buffer. The IR806 concentration was kept constant at 5 μM. (b) EEM spectrum of IR806 in the buffer. (c) EEM spectrum of IR806-HSA at 1:15 relative concentration. Please note that the scale for the z-axis in the EEM spectra is logarithmic.

The emission spectra following excitation at 16667 cm^{-1}, which is close to the excitation maximum of S_2^H, is shown as a function of HSA concentration in Figure 2a. For these measurements, the concentration of IR806 was fixed at 2 μM and the integrated emission was normalized to a constant for all the samples. For free IR806, we observe that emission from S_2^H is significantly higher and S_2^L emission is negligible. However, the emission from S_2^L increases upon IR806 binding to HSA, as can be seen in the 2 μM HSA case. The S_2^L emission shows significant enhancement with the increase of HSA concentration, along with a noticeable decrease in the S_2^H

emission. With the further increase of the HSA concentration, beyond 10 μM, we observe an even greater increase in the ratio of S_2^L to S_2^H emission, as shown in Figure 2b.

Fluorescence lifetime measurements were carried out on the IR806 and IR806-HSA solutions. Isotropic decay traces ($I_{\parallel}(t)+2I_{\perp}(t)$) of this excited state are shown in Figure 2c, which are plotted on a $\log_{10}$ scale. The fluorescence, upon laser excitation centered at 16500 cm^{-1} and detection at 14500 cm^{-1}, exhibited a biexponential decay. The deconvoluted lifetimes for the different solutions are given in Table 1. The presence of a biexponential decay indicates that a fraction of the population remains in S_2. In previous work from our group on IR144 and IR140,[4,5] we identified a change in the molecular structure associated with twisting in the polymethine chain in the S_2 state that causes a bottleneck which prevents IC to S_1. The molecules that become twisted, namely the S_2^L state, have a much slower IC to S_1, and primarily exhibit $S_2 \rightarrow S_0$ fluorescence. Therefore, the fast component τ_1 of the biexponential corresponds to a portion of the S_2 population which undergoes IC to the S_1 state, while the slow component τ_2 corresponds to a non-IC configuration that remains trapped in S_2. We rule out the possibility that the long-lived component is due to S_1 fluorescence given that the S_1 fluorescence lifetime τ_{S1} is shorter than 520 ps in the presence of HSA (see S.I. Figure S4b).

Table 1 Fluorescence lifetimes obtained from time-correlated single photon counting experiments. The time constants are as defined by the fitting equation $f(t) = a \exp(-t/\tau_1) + (1-a) \exp(-t/\tau_2)$. The anisotropy time constant R(t) is given by τ_{OR}, and the lifetime of the S1 state is given by τ_{S1}.

Sample[a]	a	τ_1 (ps)	τ_2 (ps)	τ_{avg} (ps)	τ_{OR} (ps)	τ_{S1}
IR806	0.88	273 ± 20	1138 ± 107	380 ± 31	450 ± 49	261± 3
IR806-HSA (1:1)	0.84	286 ± 3	1296 ± 22	445 ± 6	550 ± 62	305 ± 5
IR806-HSA (1:15)	0.64	293 ± 9	1363 ± 70	673 ± 31	--	505 ± 10

[*] $\tau_{avg} = a\tau_1 + (1-a)\tau_2$

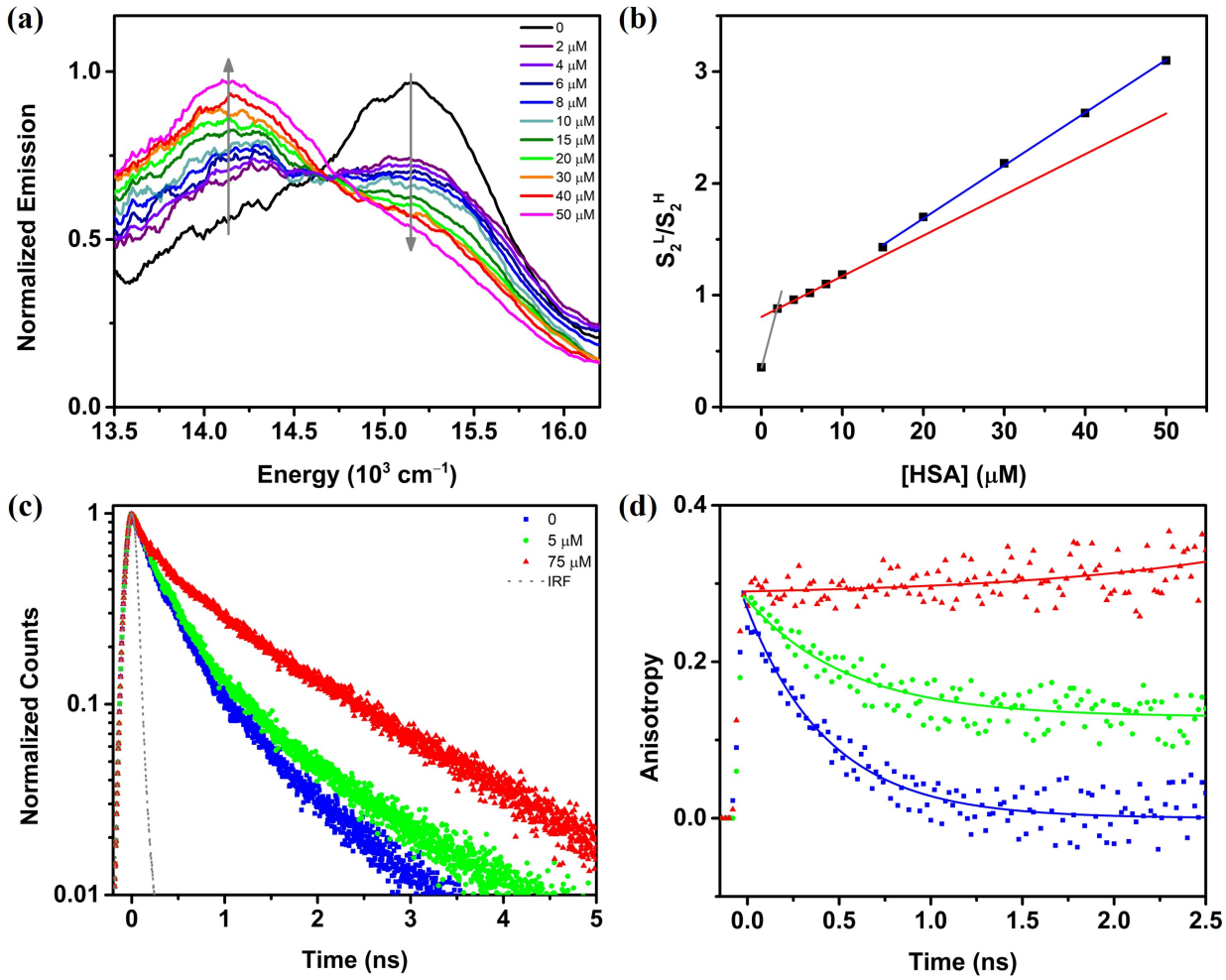

Figure 2. (a) Steady-state fluorescence of IR806 and IR806-HSA samples, with increasing HSA concentration, excited at 16667 cm^{-1}. The IR806 concentration was kept constant at 2 μM. We normalized the data to keep the integrated emission under the two fluorescence bands constant. (b) The integrated fluorescence ratio of S_2^L/S_2^H, excited at 16667 cm^{-1}, as a function of the HSA concentration. Note the difference in slope for concentrations above 10 μM, a concentration where dimerization becomes favorable. (c) The fluorescence decay of IR806 and IR806-HSA samples, with a constant IR806 concentration of 5 μM, excited at 16500 cm^{-1} and detected at 14500 cm^{-1}. (d) Rotational anisotropy decays associated with S_2 fluorescence for the samples in (c).

The experimental rotational anisotropy decays R(t), which report on the ability of molecules to reorient in solution, are shown in Figure 2d for the same solutions in Figure 2c. The decays were fitted to single exponential functions. The solution containing IR806 showed a decay of 450 ± 49 ps, the solution with 5 μM HSA showed a slower decay of 550 ± 62 ps. The solution containing 75 μM HSA showed no discernible decay within the sub-nanosecond fluorescence

lifetime. Given that reorientation time depends on molecular size, we conclude that IR806 binding to HSA slows its reorientation time, and when the concentration is high enough for the presence of dimers, it can no longer reorient during the fluorescence lifetime.

Molecular docking calculations of IR806 in HSA were carried out using AutoDockTools[41] which yielded the 10 most favorable conformations, the highest binding affinity being −9.2 kcal/mol. After analyzing the conformations, we infer that IR806 binds in the IIA subdomain of the protein primarily through hydrophobic interactions.[21–24] Figure 3a shows IR806 non-covalently bound to the hydrophobic IIA pocket of HSA, with specifically the non-polar indoline groups on one end embedded into the pocket, while the charged sulfonate group extends out of the pocket. Another iteration of docking was carried out specifically in the IIA subdomain with the objective of obtaining the most likely conformation of IR806 in HSA. The IR806 geometry, upon binding with HSA, is shown in Figure 3b which exhibits an overall twist in the polymethine chain, in comparison to the planar conformation in the unbound ground state conformation.[21,22]

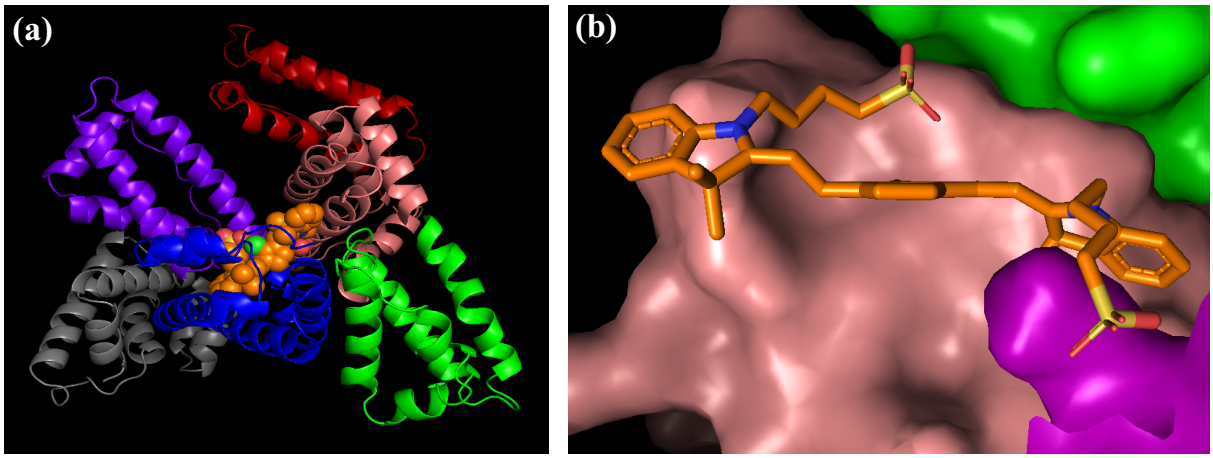

Figure 3. Molecular docking study of IR806. (a) IR806 (spheres) bound to HSA (ribbons). The different subdomains are depicted by different colors: IA - gray, IB - purple, IIA - blue, IIB - green, IIIA - salmon, and IIIB- red. The atoms of IR806 are shown by different colors as well: C - orange, Cl - green, O - red, S - yellow, and N - blue. (b) The geometry of IR806, when bound to HSA.

Electronic structure calculations using TD-DFT helped us understand the structural features of the ground and excited states of IR806. In spite of typically overestimating transition energies by almost an eV (8065 cm^{-1}) in TD-DFT calculations of cyanine dyes, the calculations are capable of depicting the intricacies of the potential energy surface trajectories accurately.[42,43] Several different ground state geometries were compared which revealed that the s-trans conformation is the most stable geometry.[44,45] The ground state geometry (S_0min) resembles a planar structure along the polymethine chain, the central cyclopentene ring, as well as the substituted aromatic indole groups on either side. The excited state optimizations were carried out to obtain the geometries responsible for the emission characteristics of IR806. Figure 4 highlights the results of our calculations with the different electronic states corresponding to the ground and excited state geometries, and the relevant transitions and the transition energies.

The vertical excitation (absorption) energy from the ground state to S_1 is 15647 cm^{-1}, which is 3146 cm^{-1} higher than the experimental S_1 maximum of 12502 cm^{-1}. The optimized first excited state, which corresponds to the vibrationally cooled conformation in the S_1 electronic state, has been labelled S_1min. The excited-state equilibrium geometry of S_1min is very similar to the geometry at the FC point of the ground state. The emission energy from S_1 is calculated at 11937 cm^{-1}, which is in excellent agreement with the experimental value of 12018 cm^{-1}.

In line with the previous calculations of IR144 and IR140, there seems to be two distinct local minima on the S_2 PES that could be resolved through our calculations.[5] The first minimum, S_2min-1, boasts a geometry that is quite similar to the S_0min and S_1min geometries, specifically in terms of the planarity of their structures. The second minimum, S_2min-2, on the contrary, displays a high degree of distortion. The polymethine chain of S_2min-2 is twisted out of plane by 103°. The emission energies estimated from our calculations are 23712 and 20728 cm^{-1} for S_2min-1 and

S_2min-2 (experimental values are 15290 and 14130 cm^{-1}), respectively. Based on qualitative agreement with experiment, the minima S_2min-1 and S_2min-2 correspond to the emissive states, S_2^H and S_2^L, in line with Laboe et al.'s work.

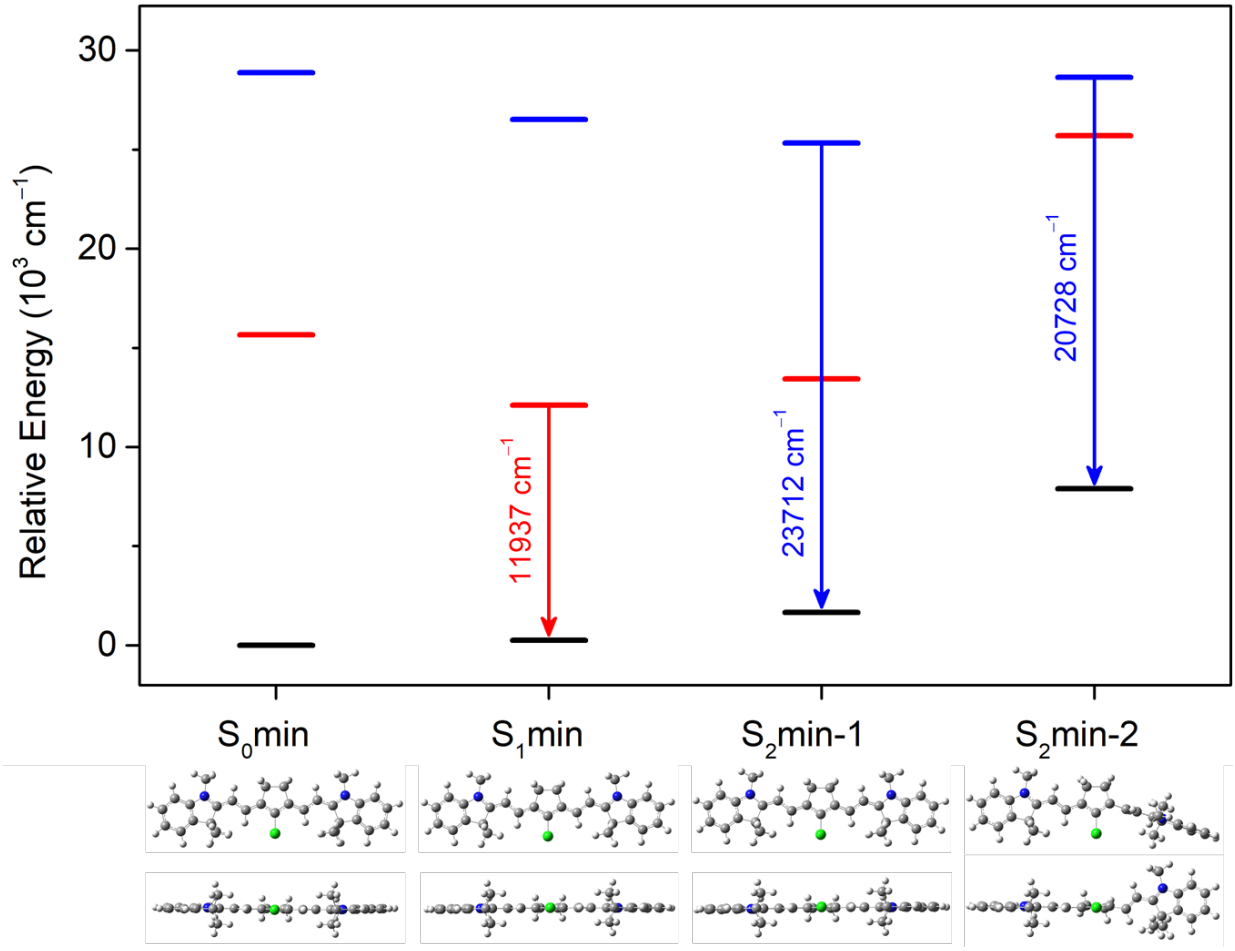

Figure 4. Results of the TD-DFT calculations showing energies for the different states corresponding to different geometries. The top row of molecular geometries depicts the molecules to be in the plane of paper while the bottom row is a visualization of the same system, with the Chlorine atom coming out of the plane of paper. The energies for S_0, S_1, and S_2 are shown in black, red, and blue, respectively.

Electronic structure calculations have helped us understand the structural features of the ground and excited states of IR806. While cis-trans isomers are known to contribute to the spectroscopy of cyanine dyes,[46,47] we did not consider the contribution of different cis-trans configurations for every carbon in the polymethine chain. The energy difference for several

different conformers, depicted in Figure S11, is given in Table S2. At room temperature we expect the EEEE conformer to be 11 times more probable than the next lowest energy conformer EEEZ. Therefore, our calculations are limited to the all-trans EEEE isomer. We examined minimum energy configurations for multiple geometries starting from different twisting angles of the carbon atoms closest to the center of the polymethine chain. We found that S_0 and S_1 always relaxed back to the planar geometry but found a configuration we call S_2^L that corresponds to a minimum with the polymethine chain twisted to 103-degrees. Emission from such a highly twisted geometry could populate the EEZE conformer but such a possibility has not been pursued here.

Non-covalent binding complex formation of HSA with IR806 manifests itself in the S_1 absorption spectrum with a red-shift as well as an increase in absorptivity (Figure S1).[21] The fact that IR806 in solution shows negative solvatochromism, i.e., a red shift in the S_1 absorption spectrum with decreasing solvent polarity, is in line with a decrease in the dipole moment upon excitation to S_1.[44] This indicates that the binding of IR806 with HSA is primarily though non-polar interactions, similar to the binding behaviors of other cyanine dyes.[21–23] The hydrophobic nature of the binding has also been captured in the docking studies of IR806 (Figure 3). Upon increasing the relative protein concentration, we see evidence of stronger protein-dye binding in the S_1 absorption spectrum of the 1:15 sample that is more red-shift in comparison to the 1:1 case (Figure 1a). The red-shift in absorption can thus be used as a gauge of protein-dye binding efficiency.

Free IR806 in solution shows two distinct absorptions from S_0 to S_2^H and S_2^L with excitation maxima at 16300 and 14900 cm^{-1}, respectively (Figure S3a). In the presence of HSA in the 1:1 mixture, the S_2 absorption band becomes wider, more intense, and shifts to a lower frequency. We associate the relative loss of intensity in the high-frequency and increase in the lower-frequency band to a loss of planar structures in the ground state, resulting from binding to

HSA. As the concentration of HSA increases, we see further shift to lower frequencies. This confirms that the bound IR806 adopts a twisted geometry in the ground state, in line with previous studies of cyanines binding with HSA.[21,22]

Free IR806 shows two conspicuous emissions from S_2^H and S_2^L. Upon binding to HSA, the S_2^L emission becomes favored, captured by the fluorescence spectra (Figure 2a) as well as the time-resolved fluorescence data (Figure 2c). Additionally, the emission from S_2^L shows significant enhancement upon increase in HSA concentration while S_2^H shows marked depletion, with a 8-fold increase in the S_2^L/S_2^H emission compared to free IR806 (Figure 2b). The fluorescence lifetime of the S_2 excited state shows a marked increase in the 75 μM HSA sample compared to the 5 μM HSA sample, because of stronger IR806 binding. The distorted configuration that IR806 adopts when bound to HSA stabilizes the 103-degree twist in the polymethine chain that characterizes the S_2^L state. This conclusion is supported by similarities of the S_2^L geometry (corresponding to S_2min-2 geometry) with the structure of the docked geometry of IR806 (Figure 3b). The enhanced emission signature can hence be used as an indication of binding.

We evaluated the spectroscopic changes in IR806 as a function of reversible HSA dimer formation. A study by Bhattacharya et al.[36] suggests that HSA dimerization becomes detectable at 10 μM HSA concentration. Chubarov et al. confirmed the reversible formation of HSA dimers, and gave the approximate equilibrium binding constant K_D~100 μM.[37] Based on those findings, we focused our study on HSA concentrations between 0 and 75 μM, while keeping a constant IR806 concentration. Based on the K_D value above, we expect dimer concentration to reach 10% when HSA concentration reaches 10 μM. First, we verified that no aggregation takes place between dye molecules upon increasing the IR806 concentration from 1 μM to 5 μM. This was confirmed from the identical line shapes of the excitation spectra. Starting with S_2 state emission

(Figure 2a), we find higher S_2^L and lower S_2^H emission, as the concentration of HSA increases. When the S_2^L/S_2^H emission ratio is plotted as a function of HSA concentration (Figure 2b), we observe a change in the slope occurring near 10 μM. We confirm the presence of dimers by the large increase in fluorescence lifetime and anisotropy decay observed for 75 μM HSA solutions (Figures 2c and d). We also looked at changes in the S_1 state spectroscopy, following excitation at its absorption maxima, for clues of dimer formation. We found that the fluorescence maxima red shifts as a function of increasing HSA concentration (Figures S6a and b) obtained at 2 and 5 μM IR806, respectively. When the shift is plotted as a function of HSA concentration, we see a change in slope near 10 μM. Similarly, when plotting the S_1 emission intensity after normalization to the emission maxima, we find a change in slope near 10 μM (Figures S8a and b). Finally, when the raw S_1 emission intensity is plotted as a function of HSA concentration (Figure S9), we find a change in slope near 10 μM (Figure S10). We attribute the spectroscopic changes observed to reversible HSA dimer formation above 10 μM HSA consistent with the findings of Bhattacharya and Chubarov.[36,37] We postulate that dimer formation leads to a more hydrophobic environment for IR806. Our findings indicate that spectroscopic changes in the S_1 and S_2 fluorescence of IR806 and perhaps other cyanines may be used as indicators for HSA oligomerization.

In this study we have explored changes in the spectroscopy of the cyanine IR806 as a function of HSA concentration in buffer solutions. Based on a spectroscopic shift in the S_1 absorption and emission, as well as changes in the S_2^L and S_2^H state emissions as a function of HSA concentration, we find that IR806 binds HSA. Protein docking calculations, together with an observed red shift of the S_1 absorption spectrum, lead us to conclude that binding takes place in the hydrophobic pocket (IIA subdomain) of HSA. From EEM spectra and electronic structure calculations, we identify the major emissive state of the IR806-HSA complex as one associated

with a 103-degree twisted geometry labeled as S_2^L. As the concentration of HSA increases above 10 μM, we find a change in the rate of spectroscopic changes affecting absorption and emission of the S_1 and S_2 states that is consistent with the formation of reversible HSA dimers. The formation of dimers was further confirmed by reorientation anisotropy measurements at low and high HSA concentrations. Findings from our study have two important implications. First, the stabilization and hence longer lived high-energy S_2 state could enable the design of more effective phototherapy agents via formation of singlet oxygen or photo-release of therapy agents. Second, the dependence on HSA concentration indicates that cyanine S_2 spectroscopy may be used to quantify the oligomerization state of HSA. This is important given the fact that HSA dimerization has been utilized as a biomarker for numerous medical conditions related to oxidative stress.

Supporting Information

Experimental Methods; Extinction Coefficients of IR806 and IR806-HSA solutions; EEM Spectra of IR806 and IR806-HSA solutions; Excitation spectra detecting S_2 emissions of IR806 and IR806-HSA solutions; S_1 emission spectra and fluorescence decay of IR806 and IR806-HSA solutions; Representative absorption, emission, and excitation spectra of IR806 and IR806-HSA solutions; Changes in the S_1 emission spectra of IR806 and IR806-HSA solutions as evidence of HSA dimer formation; Underlying raw calculations supporting the theory; Optimized geometries of IR806; Calculation of the different ground state geometries of IR806 isomers.

Notes

The authors declare no competing financial interest.

Acknowledgments

This material is based upon work supported by the National Science Foundation (Grant No. CHE1836498 to MD and BGL). BGL gratefully acknowledge startup funds from Stony Brook University. We thank Prof. Gary Blanchard (MSU) for allowing us to use his setup for obtaining additional TCSPC data. This work used the Extreme Science and Engineering Discovery Environment (XSEDE), which is supported by National Science Foundation grant number ACI-1548562.

References

(1) Kasha, M. Characterization of Electronic Transitions in Complex Molecules. *Discuss. Faraday Soc.* **1950**, *9*, 14.

(2) Kasatani, K.; Sato, H. Viscosity-Dependent Decay Dynamics of the S 2 State of Cyanine Dyes with 3, 5, and 7 Methine Units by Picosecond Fluorescence Lifetime Measurements. *Bull. Chem. Soc. Jpn.* **1996**, *69*, 3455–3460.

(3) Guarin, C. A.; Villabona-Monsalve, J. P.; López-Arteaga, R.; Peon, J. Dynamics of the Higher Lying Excited States of Cyanine Dyes. An Ultrafast Fluorescence Study. *J. Phys. Chem. B* **2013**, *117*, 7352–7362.

(4) Nairat, M.; Konar, A.; Lozovoy, V. V.; Beck, W. F.; Blanchard, G. J.; Dantus, M. Controlling S 2 Population in Cyanine Dyes Using Shaped Femtosecond Pulses. *J. Phys. Chem. A* **2016**, *120*, 1876–1885.

(5) Laboe, M.; Lahiri, J.; Mohan T. M., N.; Liang, F.; Levine, B. G.; Beck, W. F.; Dantus, M. Linear and Nonlinear Optical Processes Controlling S2 and S1 Dual Fluorescence in Cyanine Dyes. *J. Phys. Chem. A* **2021**, 10.1021/acs.jpca.1c05772.

(6) Hilderbrand, S. A.; Kelly, K. A.; Weissleder, R.; Tung, C.-H. Monofunctional Near-Infrared Fluorochromes for Imaging Applications. *Bioconjug. Chem.* **2005**, *16*, 1275–1281.

(7) Shi, C.; Wu, J. B.; Pan, D. Review on Near-Infrared Heptamethine Cyanine Dyes as Theranostic Agents for Tumor Imaging, Targeting, and Photodynamic Therapy. *J. Biomed. Opt.* **2016**, *21*, 050901.

(8) Li, Y.; Zhou, Y.; Yue, X.; Dai, Z. Cyanine Conjugates in Cancer Theranostics. *Bioact. Mater.* **2021**, *6*, 794–809.

(9) Bilici, K.; Cetin, S.; Aydındogan, E.; Yagci Acar, H.; Kolemen, S. Recent Advances in Cyanine-Based Phototherapy Agents. *Front. Chem.* **2021**, *9*, 380–387.

(10) Gorka, A. P.; Nani, R. R.; Zhu, J.; Mackem, S.; Schnermann, M. J. A Near-IR Uncaging Strategy Based on Cyanine Photochemistry. *J. Am. Chem. Soc.* **2014**, *136*, 14153–14159.

(11) Nani, R. R.; Gorka, A. P.; Nagaya, T.; Kobayashi, H.; Schnermann, M. J. Near-IR Light-Mediated Cleavage of Antibody–Drug Conjugates Using Cyanine Photocages. *Angew. Chemie Int. Ed.* **2015**, *54*, 13635–13638.

(12) Nani, R. R.; Gorka, A. P.; Nagaya, T.; Yamamoto, T.; Ivanic, J.; Kobayashi, H.; Schnermann, M. J. In Vivo Activation of Duocarmycin–Antibody Conjugates by Near-Infrared Light. *ACS Cent. Sci.* **2017**, *3*, 329–337.

(13) Shi, L.; Yan, C.; Guo, Z.; Chi, W.; Wei, J.; Liu, W.; Liu, X.; Tian, H.; Zhu, W. H. De Novo Strategy with Engineering Anti-Kasha/Kasha Fluorophores Enables Reliable Ratiometric Quantification of Biomolecules. *Nat. Commun.* **2020**, *11*, 1–3.

(14) Demchenko, A. P.; Tomin, V. I.; Chou, P.-T. Breaking the Kasha Rule for More Efficient Photochemistry. *Chem. Rev.* **2017**, *117*, 13353–13381.

(15) Rodríguez-Romero, J.; Guarin, C. A.; Arroyo-Pieck, A.; Gutiérrez-Arzaluz, L.; López-Arteaga, R.; Cortés-Guzmán, F.; Navarro, P.; Peon, J. Fluorophore Release from a Polymethinic Photoremovable Protecting Group Through a Nonlinear Optical Process. *ChemPhotoChem* **2017**, *1*, 397–407.

(16) Cherrick, G. R.; Stein, S. W.; Leevy, C. M.; Davidson, C. S. Indocyanine Green: Observations on Its Physical Properties, Plasma Decay, and Hepatic Extraction. *J. Clin. Invest.* **1960**, *39*, 592–600.

(17) Alander, J. T.; Kaartinen, I.; Laakso, A.; Pätilä, T.; Spillmann, T.; Tuchin, V. V.; Venermo, M.; Välisuo, P. A Review of Indocyanine Green Fluorescent Imaging in Surgery. *Int. J. Biomed. Imaging* **2012**, *2012*.

(18) Boni, L.; David, G.; Mangano, A.; Dionigi, G.; Rausei, S.; Spampatti, S.; Cassinotti, E.; Fingerhut, A. Clinical Applications of Indocyanine Green (ICG) Enhanced Fluorescence in Laparoscopic Surgery. *Surg. Endosc.* **2015**, *29*, 2046–2055.

(19) Berezin, M. Y.; Lee, H.; Akers, W.; Nikiforovich, G.; Achilefu, S. Ratiometric Analysis of Fluorescence Lifetime for Probing Binding Sites in Albumin with Near-Infrared Fluorescent Molecular Probes. *Photochem. Photobiol.* **2007**, *83*, 1371–1378.

(20) Awasthi, K.; Nishimura, G. Modification of Near-Infrared Cyanine Dyes by Serum Albumin Protein. *Photochem. Photobiol. Sci.* **2011**, *10*, 461–463.

(21) Nairat, M.; Konar, A.; Kaniecki, M.; Lozovoya, V. V.; Dantus, M. Investigating the Role

of Human Serum Albumin Protein Pocket on the Excited State Dynamics of Indocyanine Green Using Shaped Femtosecond Laser Pulses. *Phys. Chem. Chem. Phys.* **2015**, *17*, 5872–5877.

(22) Tian, R.; Zeng, Q.; Zhu, S.; Lau, J.; Chandra, S.; Ertsey, R.; Hettie, K. S.; Teraphongphom, T.; Hu, Z.; Niu, G.; Kiesewetter, D. O.; Sun, H.; Zhang, X.; Antaris, A. L.; Brooks, B. R.; Chen, X. Albumin-Chaperoned Cyanine Dye Yields Superbright NIR-II Fluorophore with Enhanced Pharmacokinetics. *Sci. Adv.* **2019**, *5*, 1–12.

(23) Du, B.; Qu, C.; Qian, K.; Ren, Y.; Li, Y.; Cui, X.; He, S.; Wu, Y.; Ko, T.; Liu, R.; Li, X.; Li, Y.; Cheng, Z. An IR820 Dye–Protein Complex for Second Near-Infrared Window and Photoacoustic Imaging. *Adv. Opt. Mater.* **2020**, *8*, 1901471.

(24) He, X. M.; Carter, D. C. Atomic Structure and Chemistry of Human Serum Albumin. *Nature* **1992**, *358*, 209–215.

(25) Peters Jr., T. *All About Albumin*, 1st Editio.; Elsevier: Orlando, Florida, 1995.

(26) Sugio, S.; Kashima, A.; Mochizuki, S.; Noda, M.; Kobayashi, K. Crystal Structure of Human Serum Albumin at 2.5 Å Resolution. *Protein Eng. Des. Sel.* **1999**, *12*, 439–446.

(27) Kunkel, H. G.; Labby, D. H.; Ahrens, E. H.; Shank, R. E.; Hoagland, C. L. The Use of Concentrated Human Serum Albumin in the Treatment of Cirrhosis of the Liver 1. *J. Clin. Invest.* **1948**, *27*, 305–319.

(28) Thorn, G. W.; Armstrong, S. H. Chemical, Clinical, and Immunological Studies on the Products of Human Plasma Fractionation; the Use of Salt-Poor Concentrated Human Serum Albumin Solution in the Treatment of Chronic Bright's Disease. *J. Clin. Invest.*

1945, *24*, 802–828.

(29) Caraceni, P.; Tufoni, M.; Bonavita, M. E. Clinical Use of Albumin. *Blood Transfus.* **2013**, *11*, 20894.

(30) Taverna, M.; Marie, A.-L.; Mira, J.-P.; Guidet, B. Specific Antioxidant Properties of Human Serum Albumin. *Ann. Intensive Care* **2013**, *3*, 4.

(31) Sudlow, G.; Birkett, D. J.; Wade, D. N. The Characterization of Two Specific Drug Binding Sites on Human Serum Albumin. *Mol. Pharmacol.* **1975**, *11*, 824–832.

(32) Sudlow, G.; Birkett, D. J.; Wade, D. N. Albumin. *Mol. Pharmacol.* **1976**, *12*, 1052–1061.

(33) Berde, C. B.; Hudson, B. S.; Simoni, R. D.; Sklar, L. A. Human Serum Albumin. Spectroscopic Studies of Binding and Proximity Relationships for Fatty Acids and Bilirubin. *J. Biol. Chem.* **1979**, *254*, 391–400.

(34) Ferrer, M. L.; Duchowicz, R.; Carrasco, B.; De La Torre, J. G.; Acuña, A. U. The Conformation of Serum Albumin in Solution: A Combined Phosphorescence Depolarization-Hydrodynamic Modeling Study. *Biophys. J.* **2001**, *80*, 2422–2430.

(35) Akdogan, Y.; Reichenwallner, J.; Hinderberger, D. Evidence for Water-Tuned Structural Differences in Proteins: An Approach Emphasizing Variations in Local Hydrophilicity. *PLoS One* **2012**, *7*, e45681.

(36) Bhattacharya, A.; Prajapati, R.; Chatterjee, S.; Mukherjee, T. K. Concentration-Dependent Reversible Self-Oligomerization of Serum Albumins through Intermolecular β-Sheet Formation. *Langmuir* **2014**, *30*, 14894–14904.

(37) Chubarov, A.; Spitsyna, A.; Krumkacheva, O.; Mitin, D.; Suvorov, D.; Tormyshev, V.;

Fedin, M.; Bowman, M. K.; Bagryanskaya, E. Reversible Dimerization of Human Serum Albumin. *Molecules* **2021**, *26*, 108.

(38) Ogasawara, Y.; Namai, T.; Togawa, T.; Ishii, K. Formation of Albumin Dimers Induced by Exposure to Peroxides in Human Plasma: A Possible Biomarker for Oxidative Stress. *Biochem. Biophys. Res. Commun.* **2006**, *340*, 353–358.

(39) Naldi, M.; Baldassarre, M.; Nati, M.; Laggetta, M.; Giannone, F. A.; Domenicali, M.; Bernardi, M.; Caraceni, P.; Bertucci, C. Mass Spectrometric Characterization of Human Serum Albumin Dimer: A New Potential Biomarker in Chronic Liver Diseases. *J. Pharm. Biomed. Anal.* **2015**, *112*, 169–175.

(40) Zhong, D.; Douhal, A.; Zewail, A. H. Femtosecond Studies of Protein-Ligand Hydrophobic Binding and Dynamics: Human Serum Albumin. *Proc. Natl. Acad. Sci. U. S. A.* **2000**, *97*, 14056–14061.

(41) Sanner, M. F. Python: A Programming Language for Software Integration and Development. *J. Mol. Graph. Model.* **1999**, *17*, 57–61.

(42) Adamo, C.; Jacquemin, D. The Calculations of Excited-State Properties with Time-Dependent Density Functional Theory. *Chem. Soc. Rev.* **2013**, *42*, 845–856.

(43) Le Guennic, B.; Jacquemin, D. Taking Up the Cyanine Challenge with Quantum Tools. *Acc. Chem. Res.* **2015**, *48*, 530–537.

(44) Nairat, M.; Webb, M.; Esch, M. P.; Lozovoy, V. V; Levine, B. G.; Dantus, M. Time-Resolved Signatures across the Intramolecular Response in Substituted Cyanine Dyes. *Phys. Chem. Chem. Phys.* **2017**, *19*, 14085–14095.

(45) Hervé, M.; Brédy, R.; Karras, G.; Concina, B.; Brown, J.; Allouche, A.-R.; Lépine, F.; Compagnon, I. On-the-Fly Femtosecond Action Spectroscopy of Charged Cyanine Dyes: Electronic Structure versus Geometry. *J. Phys. Chem. Lett.* **2019**, *10*, 2300–2305.

(46) Wang, D.; Jiang, H.; Yang, H.; Liu, C.; Gong, Q.; Xiang, J.; Xu, G. Investigation on Photoexcited Dynamics of IR-140 Dye in Ethanol by Femtosecond Supercontinuum-Probing Technique. *J. Opt. A Pure Appl. Opt.* **2002**, *4*, 155–159.

(47) Silori, Y.; Seliya, P.; De, A. K. Ultrafast Excited-State Dynamics of Tricarbocyanine Dyes Probed by Two-Dimensional Electronic Spectroscopy: Polar Solvation vs Photoisomerization. *J. Phys. Chem. B* **2020**, *124*, 6825–6834.